PAPER

Check for updates

Pen direct writing of SERRS-based lateral flow assays for detection of penicillin G in milk†

Alida Russo, [ID] [a] Simone Cavalera, [ID] [b] Richard Murray, [ID] [a] Pierre Lovera,[a] Aidan Quinn, [ID] [a] Laura Anfossi [ID] [b] and Daniela Iacopino [ID] *[a]

Direct pen writing offers versatile opportunities for development of low-cost tests for point-of-care applications. In this work a lateral flow immunoassay (LFIA) test was fabricated by hand "writing" immunoprobes onto hand-cut nitrocellulose strips with a commercial fountain pen. The qualitative capabilities of the test were extended by addition of a Raman reporter and consequent design and fabrication of a Surface Enhanced Resonant Raman Scattering (SERRS)-LFIA test. As proof-of-concept, dual detection of penicillin G was achieved in milk with a visual LOD of 20 ppm and a dynamic range of 0.03–97.5 ppm. Evaluation against equivalent tests performed with conventionally prepared LFIA strips showed comparable results, thus demonstrating the validity of the test. These results demonstrate the potential for further decrease in cost and consequent broader use of LFIA tests in remote regions and resource-limited environments.

Introduction

Direct writing of bioassays and biosensors on paper has recently emerged as a versatile, precise and sensitive technique for low-cost point-of-care (POC) applications.[1–3] Such methodology makes use of conventional writing tools, such as commercial rollerball or ballpoint pens, to pattern conductive or bioactive inks on paper-based substrates for electrochemical or colorimetric assay development.[4–7] This can be implemented by simple handwriting of individual assays, but can extend to high throughput fabrication by incorporation of writing pens into automated, customised pen-plotter systems.[8–10] Direct writing methods benefit from the use of readily available materials and easy fabrication techniques and can be integrated with microfluidics (paper cut, permanent markers, wax pens/printers) to design and deliver low-cost, multiplexed, disposable, scalable and portable assays.[11–13] These characteristics are particularly attractive to implement POC tests in remote regions and resource-limited environments.

Lateral flow immunoassay (LFIA) is a very popular POC test, extensively used for medical, environmental and food quality analysis, due to its low cost, ease of use and long shelf stability.[14] The working principle of the most commonly used LFIA is the visual detection of coloured lines on a nitrocellulose membrane. The line formation is caused by capillary migration of

biomolecules, labelled with gold nanoparticles (Au NPs), on the membrane, where relevant immunoprobes are immobilized. The most popular LFIA format is the sandwich assay, whereby two red lines, corresponding to the test (T) and control (C) lines, are formed for a positive test. However, for the analysis of small molecules, a competitive assay format must be used, whereby only one red line (the C line) is generated for a positive test, while the presence of both T and C lines indicates a negative response. LFIA assays are generally used as screening tests, based on the qualitative nature of the generated colorimetric response. However, for many clinical and food safety analyses, LFIAs are limited by relatively low sensitivity and the lack of quantification.

Recently, dual detection methods have emerged where the LFIA naked-eye colorimetric readout is combined with other techniques to perform quantitative detection and increase sensitivity.[15–18]

Surface Enhanced Raman Scattering (SERS)-based LFIA assays have been shown to enable sensitive and quantitative detection of analytes like pathogens and bacteria in complex matrices, ranging from human serum to milk.[19–22] SERS is a phenomenon where the Raman signal of an analyte is largely enhanced (up to a factor 10^{11} to 10^{12}) by its close proximity to a nanostructured metal surface.[23] The enhancement arises from a combination of electromagnetic effects, associated with the excitation of the nanostructured surface by the incident laser local surface plasmon resonance (LSPR), and chemical effects associated with electron transfer transitions occurring between the analyte and the nanostructured surface.[23]

Furthermore, if the electronic transition energy of the analyte under investigation matches the excitation wavelength of the incident laser, an additional "molecular effect" arises and the technique becomes known as Surface Enhanced Resonance Raman Scattering (SERRS).[24]

[a]*Tyndall National Institute, University College Cork, Lee Maltings Complex, Dyke Parade, T12R5CP, Cork, Ireland. E-mail: daniela.iacopino@tyndall.ie*

[b]*Department of Chemistry, University of Turin, Via P. Giuria 5, 10125, Turin, Italy*

In a SERS-LFIA assay format, the Au NPs are also modified with a Raman reporter in addition to the antibody of conventional LFIA tests. Upon attachment of the Au NP immunoprobes to the T line, a strong SERS signal is generated, which is directly (sandwich assay) or inversely (competitive assay) proportional to the concentration of the target analyte. Recently, successful examples of SERS-LFIA assays have been reported for detection of antibiotics in food,[25] viruses,[26,27] bacteria,[28] toxins,[29] biomarkers.[30,31] In parallel, the use of commercial pens to write LFIA assays has been recently demonstrated.[3] Specifically, by using multicolour commercial BIC© pens to write nucleic probes and nucleic-acid modified Au NPs, Han *et al.* demonstrated POC detection of human immunodeficiency virus type (HIV-1). The method drastically reduced the cost of traditional LFIA tests fabrication and showed the potential of such "do-it-yourself" (DIY) tests for use in regions or settings with limited laboratory facilities and trained operators.

On food safety, our interest was directed towards antibiotics, which still play a major role in veterinary medicine, despite falling usage across Europe (25 countries) by 53% on average between 2011 and 2022.[32] In particular though, their use for food animals could lead to the presence of residuals in meat or milk.[33] Among antibiotics, in 2022, penicillins were the highest selling class accounting for 32.7% (ref. 32) of overall sales (considering 31 countries), and in Ireland were the second best-selling class for 26.3% (ref. 34) over veterinary antibiotics supplied.

Different techniques have been used for detection of penicillins, such as liquid chromatography,[35] liquid chromatography-tandem mass spectrometry,[36] MALDI-TOF mass spectrometry,[37] microbial tests,[38] surface plasmon resonance sensors,[39] magnetic immunodetection,[40] and amperometric sensors.[41]

In this paper, we have developed a novel pen-written SERRS-LFIA assay by using a commercial fountain pen to write T and C lines onto hand-assembled LFIA test pads. The viability of the assay was demonstrated by the detection of the antibiotic penicillin G (benzylpenicillin) in milk.

Antibody directed to penicillin and Raman reporter Rhodamine isothiocyanate (RhITC) were crafted on the surface of Au NPs and were used to achieve a dual SERRS-colorimetric detection. In spite of the simplicity of fabrication, the assay showed sensitivity comparable to LFIAs fabricated by costly traditional methods. The combination of colorimetric and SERRS detection allowed quantification of penicillin in spiked milk samples. This work shows the applicability of SERRS-LFIA methods for food safety and control and opens the way to low-cost DIY methods for POC clinical, food safety, security, and environmental applications.

Experimental section/materials and methods

Immunoreagents, chemicals and materials

Tetrachloroauric(III) acid, bovine serum albumin (BSA), Rhodamine B isothiocyanate (RhITC), penicillin G sodium salt,

antirabbit immunoglobulins (goat polyclonal antibodies), Tween 20 and all salts for buffer preparation were purchased from Sigma-Aldrich (Arklow, Ireland). All solutions were prepared using Milli-Q water (resistivity 18.2 MΩ cm).

The antigen penicillin–BSA was purchased from Fitzgerald industries International (Acton, MA, USA). The anti-ampicillin antibody (rabbit polyclonal immunoglobulin obtained by ammonium sulphate precipitation, anti-P) was produced by Davids Biotechnologies after immunization with ampicillin–BSA immunogen synthesised as previously reported by Cliquet *et al.*[42] with minor modifications. Details of the synthesis are described in ESI.† Nitrocellulose membranes, sample and adsorbent pad, and glass fiber conjugate pad were obtained from Advanced Microdevices Pvt. Ltd (Ambala Cantt, India). The Parker fountain pen and its standard ink cartridges have been purchased from "Cork Art Supplies" shop (Cork, Ireland).

Characterization

UV-vis spectra were acquired using an Agilent/HP 8453 UV-vis Spectrophotometer (190–1100 nm, spectral bandwidth 1 nm). Scanning electron microscopy images were obtained with a Zeiss Supra scanning electron microscope (SEM) operating at accelerating voltages in the range of 5–8 kV. Nanoparticle SEM images were obtained from diluted solutions deposited on n-doped Si wafers, whereas nitrocellulose samples were coated with ~10 nm film of AuPd (90% Au, 10% Pd) prior to SEM imaging. The hydrodynamic diameter of Au NPs aqueous solutions, bare and modified using an optical density (OD) range 0.8–1, was obtained using a Zetasizer instrument (Zetasizer Nano-ZS, Malvern Instruments, Malvern Panalytical, UK) based on dynamic light scattering (DLS) technique. Same instrument was used for acquiring the surface charge of Au NPs aqueous solutions, based on zeta-potential by electrophoretic light scattering (ELS).

All Raman measurements were carried out using a Horiba-Xplora Raman microscope equipped with a 70 mW 532 nm laser (1–10% laser power, 10–60 s, 10–50× objectives). The spectra obtained were processed and analysed using the software LabSpec 6 and OriginPRO 2022, respectively.

Synthesis of Au NPs

Au NPs were synthesised through Turkevich–Frens[43,44] citrate reduction method from tetrachloroauric(III) acid as described by Anfossi *et al.*[45] Briefly, 1 ml of sodium citrate 1% w/v was added to 100 ml of a 0.01% w/v solution of tetrachloroauric acid, under boiling and vigorous stirring. The solution colour changed slowly from light yellow to brilliant red, indicating the formation of Au NPs, passing through grey, black and purple colour. After cooling to room temperature, the colloidal solution was stored at 4 °C for further use.

Preparation of Raman reporter labelled immunogold nanoparticles

To prepare a Raman active probe, Raman reporter RhITC was adsorbed onto the surface of Au NPs as described by Wang *et al.*[19] with slight modifications. In particular, 10 μl of a 0.1 mM

RhITC solution in ethanol (96% v/v) was mixed with 10 ml of Au NPs solution (optical density OD ~ 1). The mixture was stirred for about 3 h, centrifuged at 10 000 rpm for 10 min to remove excess reagents and re-suspended in water. Before proceeding with antibody conjugation, the pH of the RhITC–Au NPs solution was adjusted to pH 8, using a sodium carbonate-sodium bicarbonate buffer (50 mM, pH 9.6).

Antibody conjugation to Au NPs was achieved through passive adsorption of proteins onto the surface of the NPs as reported by Anfossi *et al.*[46] with some modifications. Briefly, 4 µg of anti-P was added to 1 ml of Au NPs solution and 100 µl of borate buffer (BB) 20 mM pH 8, and incubated for 30 min at 37 °C. After addition of 100 µl of BB supplemented with 1% w/v BSA, a second incubation was performed for 10 min. The mixture was then centrifuged for 10 min at 25 °C at 16 100 rcf. The optimal amount for each mL of Au NP (OD ~ 1) was defined based on the flocculation stress test as described in the Results and discussion section. The pellet was washed twice by resuspension in 0.1% w/v BSA BB and in BB containing 1% w/v BSA, 2% w/v sucrose, 0.25% v/v Tween 20 and 0.02% w/v sodium azide. The final RhITC–antiP–Au NPs pellet was stored at 4 °C until further use.

Fabrication of lateral flow immunoassay (LFIA) strips

The SERRS-LFIA strips consisted of four main components: a sample pad, a conjugate pad, a nitrocellulose membrane, and an adsorbent pad. Each component was fixed on a PVC adhesive backing layer and the different components were overlapped to ensure the solution flow as shown in Fig. 3. The T and C lines were deposited onto the nitrocellulose membrane using a fountain pen filled with the respective solutions. The T line was constituted by 1 mg ml^{-1} of capturing antigen (penicillin–BSA), while the C line contained 0.7 mg ml^{-1} of anti-rabbit antibody. Both reagents were diluted in phosphate buffer (PB) 20 mM pH 7.4. The conjugate pad, previously treated with BB containing 1% w/v BSA, 2% w/v sucrose, 0.25% v/v Tween 20 and 0.02% w/v sodium azide and dried for 1 h at 60 °C, was saturated with the solution of RhITC–antiP–Au NPs (OD 3) and dried at room temperature for at least 3 hours. The most appropriate optical density of the signal reported was defined as described in ESI.†

The nitrocellulose membranes were dried at 37 °C for 1 hour and then laminated with sample, conjugate, and adsorbent pads. The assembled membranes were cut into 4 mm width strips, inserted into rigid plastic cassettes and stored in plastic bags until further use.

Results were qualitatively compared by visual inspection (naked eye). Photographs of the strips were taken after 15 min after the test completion, using a smartphone camera (48 MP). To ensure reproducible illumination conditions, the strips were photographed inside a 3D printed chamber illuminated with 9 LED lights (see Fig. S2†).

Milk samples preparation for SERRS-LFIA

Fresh milk samples, farmed and produced in the Republic of Ireland, were purchased from a local company, approved by the National Dairy Council. Milk was diluted 1 : 1 with a buffer solution (PB 20 mM pH 7.4, 0.2% v/v Tween 20) and it was spiked with the appropriate amount of standard solution of penicillin G (500, 200, 20, 2, 0.2, 0.02, 0.002 ppm). The dilution was chosen as described in ESI† to minimize the treatment of the matrix.

SERRS spectra acquisition

Nine SERRS spectra for each concentration were acquired across a 50 × 80 µm grid selected in the middle of each test line.

The spectra were acquired using 532 nm laser with a power of 0.7 mW in 10 s per spectrum and 50× objective. The data obtained were assessed to compare the intensity of the reference peak for the RhITC, 1647 cm^{-1},[47] at different concentrations of penicillin G.

The smoothing and baseline subtraction have been processed though the software LabSpec 6 using a 1st order polynomial fitting and 1st order interpolative baseline subtraction. The peaks were fitted using Lorentzian lineshapes in OriginPRO 22.

Results and discussion

Direct pen writing

Commercial pens were investigated for the development of the DIY direct writing methods, as alternative to the use of automatic dispensers, as a route to reduce the cost of LFIAs and to widen the usability to different analytical settings. Different commercial pens were used, including ballpoint BIC©, gel, fountain and felt tip pens (see Table S1†) on different paper substrates. Customized cleaning, filling, and writing protocols were developed for the different pens, as described in the ESI.† In all cases, writing was performed by hand, considering the pressure exerted by the writing hand and the fragility of the writing substrate. In order to visually inspect the quality of written lines, coloured dyes or concentrated solutions of Au NPs (OD ~ 10) were used to test different pens. A comparison of written lines obtained with three different pens is shown in Fig. S3.† Following this initial screening phase, fountain pens were selected. This choice was dictated by the uniformity of lines formed on the nitrocellulose membrane and the commercial availability of empty cartridges, which allowed prompt use without lengthy cleaning procedures.

Fig. 1 shows digital photographs and optical microscopy images of pen writings of Au NPs concentrated solution (OD ~ 10) on 3 different substrates: glass fiber (Fig. 1a and d), printer paper (Fig. 1b and e) and nitrocellulose (Fig. 1c and f). All these written lines were performed with a PARKER© Vector fountain pen (Fig. 1g), the pen chosen for the final purpose of this work, which contained a removable reservoir for the aqueous ink and dispensed ink through the nib, *via* a combination of gravity and capillary action.[48] Sequential overlay of written lines (1 to 10 passes per line) were performed on the diverse substrates, as shown in Fig. 1a–c, in order to select the optimum line width and coloration. For all lines, a darker colour but also a certain degree of line broadening was observed as the writing steps
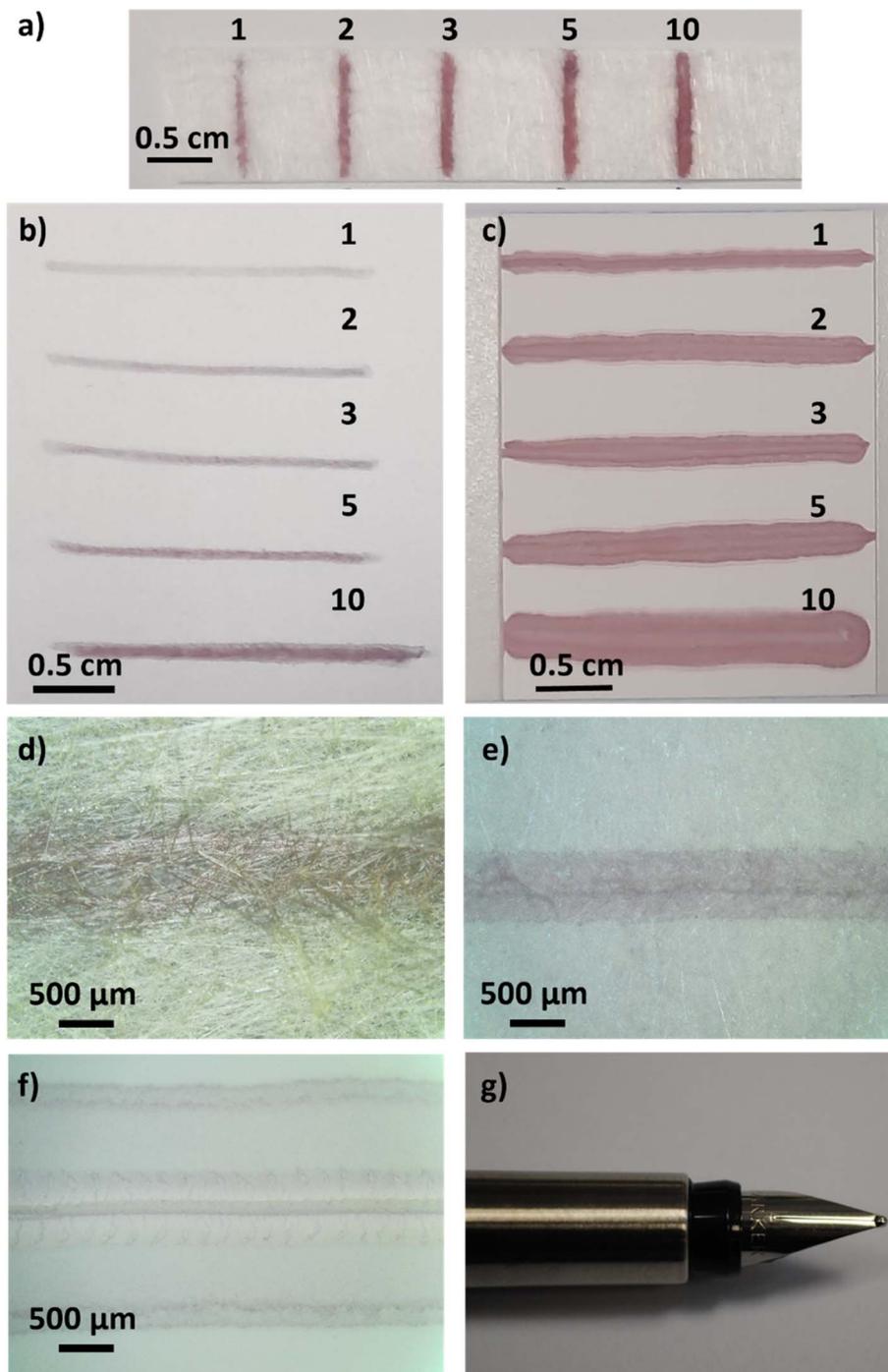
Fig. 1   Digital photographs and optical microscopy images of multistep writings of concentrated Au NPs on different substrates. Glass fiber: (a) digital and (d) optical microscopy image; printer paper: (b) digital and (e) optical microscopy image; nitrocellulose: (c) digital and (f) optical microscopy image. (g) Photograph of the fountain pen (PARKER© Vector) used in this work.

increased from 1 to 10. The microscopy images of Fig. 1d–f show the homogeneity of particle deposition in different substrates, following one step of writing. The glass fiber pad (Fig. 1d, line width $\sim$ 685 µm) displayed good homogeneity of colour; this good colour distribution suggested that the fountain pen could be also used for the deposition of the conjugate in the LFIA test, allowing a straight-line deposition of the

modified nanoparticles. However, for this work, a pad saturation approach was used, as discussed in the Experimental section. The printer paper (Fig. 1e, line width $\sim$ 630 µm) displayed a darker line mark within the coloured line, associated to the scraping of the nib on the paper. In the nitrocellulose (Fig. 1f, line width: $\sim$1440 µm) the furrow left by the nib became more visible with the increase in the number of writing steps,

due to the fragility of the substrate, especially rewriting on the same path. Also, the broadening of the line compared with the line width obtained with other substrates was evident, and likely caused by the porosity of the nitrocellulose substrate.

Considering the application in LFIA, optimization of the writing in the nitrocellulose membrane was necessary for the deposition of test and control lines. Since the lines were hand-written, different pressures applied on the surface and hand positions were tried to allow a correct deposition of the reagents, without any damage. Fig. 2a–c shows a scheme of writing, a digital photograph and a optical microscopy image of lines written on nitrocellulose by fountain pen using a Patent Blue V dye. Different lines with different hand pressures were written without damage of the nitrocellulose membrane. In all cases, the dye distribution appeared uniform under microscope illumination. Fig. 2d shows the scheme of writing of a secondary antibody (0.25 mg ml^{-1} in PB) on the nitrocellulose via fountain pen. The digital photograph (Fig. 2e) shows a pen written line, equivalent to a C line, and the colouration of the same line obtained after Au NPs migration and attachment to it. The homogenous and strong colouration of the line was indicative of the successful immobilization of secondary antibody by pen writing on the nitrocellulose.

In order to evaluate the validity of the developed method, a LFIA test for detection of penicillin G in milk was targeted. Furthermore, a Raman reporter was also incorporated in order to widen the scope of application and add quantitative capabilities. Fig. 3a shows details of reagents and materials used in this SERRS-LFIA test, whereby the cartridges of commercial pens were loaded with penicillin–BSA and anti-rabbit antibody solutions to write T and C lines, respectively. RhITC–antiP–Au NPs were deposited by saturation of the glass–fiber conjugate pad. Since antibiotics are small molecules, a competitive format was chosen for the detection of penicillin G (Fig. 3b). This relies on the competition between the target analyte penicillin and the antigen penicillin–BSA deposited on the T line for the binding sites of the antibody grafted on the Au NPs. As shown in the Fig. 3b, the analyte solution flows through the sample pad and the conjugate pad, resuspending the RhITC–antiP–Au NPs and migrating through the nitrocellulose membrane by capillary action. In absence of target penicillin G, the RhITC–antiP–Au NPs attach to both the T and C lines, giving two red lines as negative test response. However, if penicillin G is present in the analyte solution, the RhITC–antiP–Au NPs will preferentially bind it, ending their flow in the adsorption pad at the end of the strip. The free RhITC–antiP–Au NPs, which fail to bind to penicillin, are captured by the T line, resulting in a visible red coloured line. The excess RhITC–antiP–Au NPs will bind the C line, confirming the working principles of the test. The higher the penicillin concentration, the fewer labelled NPs are available to bind to the test line, decreasing its colour intensity. This results in a coloured C line and
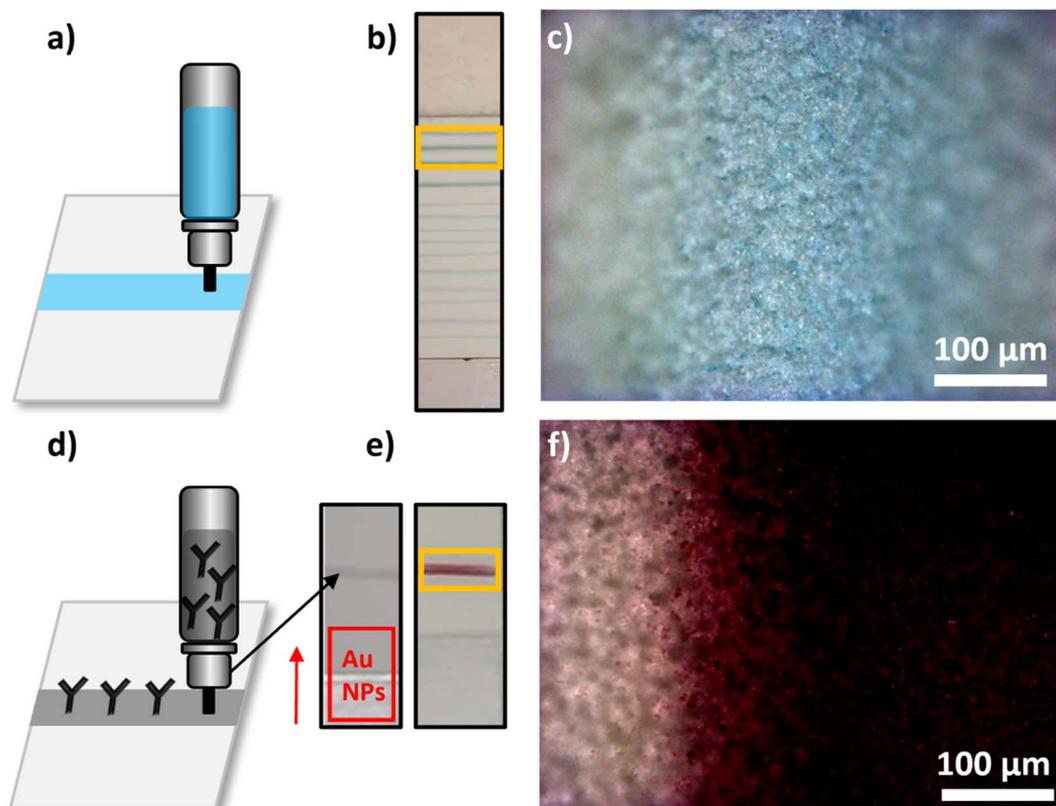

Fig. 2 (a) Scheme of the writing by fountain pen on a paper substrate with Patent Blue V dye. (b) Digital picture of the nitrocellulose written with different pressures with the fountain pen loaded with the blue dye. (c) Optical microscopy image of a line written by fountain pen with blue dye. (d) Scheme of the writing by fountain pen loaded with secondary antibody solution for development of LFIA strips. (e) Digital photograph and (f) optical microscopy image of line written manually by fountain pen on a developed test.
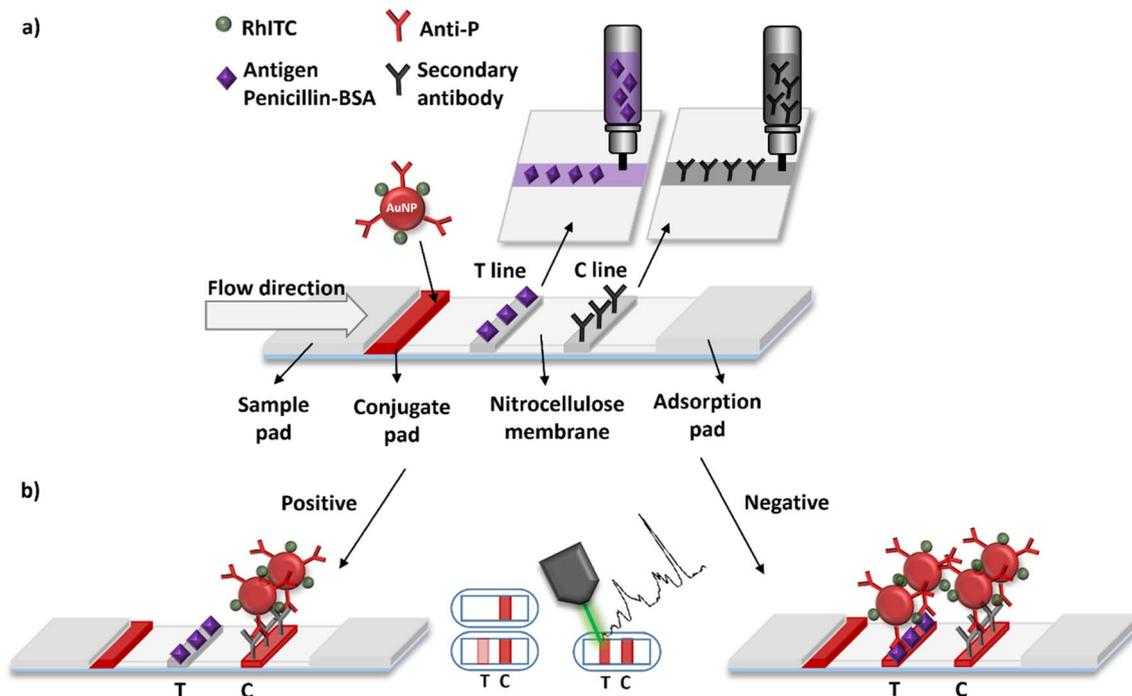
Fig. 3 (a) Schematic representation of the LFIA test fabrication process with details on the material used; (b) principle of a competitive SERRS-based LFIA.

a transparent (or a possible faint red coloured) T line for a positive test response. Therefore, the colour of the test line is inversely dependent on the amount of penicillin G in the sample, as shown in Fig. 3b. In this test in addition to this visual response, a SERRS response can be measured (Fig. 3b) by recording the SERRS spectra generated on the T and C lines generated by the Raman reporter (RhITC) grafted onto the Au NPs. The SERRS response of the LFIA test highly complements the visual response and provides enhanced sensitivity and quantitative information.

LFIA immunoprobes preparation and characterisation

Fig. 4a shows a schematic illustration of the Au NPs used in this work, obtained by reduction of tetrachloroauric(III) acid mediated by citrate, and whose surface was modified with target anti-P and Raman reporter RhITC for subsequent SERRS-LFIA analysis. The Au NPs showed spherical shape with an average size of 24.5 nm $\pm$ 4.9 nm (see Fig. 4c and inset). The UV-vis spectrum of Au NPs was characterised by a LSPR band centred at 525 nm (see Fig. 4b, black line). The encoding of the Raman reporter was carried out by simple mixing of the RhITC solution with the colloidal solution of Au NPs. The presence of sulphur in the isothiocyanate group of the RhITC allowed its chemical binding to the NPs. Raman spectroscopy was performed to verify successful attachment of RhITC to the Au NPs. Fig. 4d shows the SERRS spectrum of RhITC–Au NPs deposited on a glass slide (red line), following two cycles of centrifugation-redispersion in order to remove excess unbound Raman reporter.

The spectrum showed the characteristic peaks of RhITC at 1647 cm^{-1}, 1563 cm^{-1}, 1529 cm^{-1}, 1508 cm^{-1} and 1358 cm^{-1} (aromatic C–C stretching), 1281 cm^{-1} (C–C bridge-bands stretching) and 1200 cm^{-1} (aromatic C–H bending).[49] The intensity of the Raman RhITC bands was enhanced by a combination of an electromagnetic enhancement, associated to the excitation of the Au NPs plasmon resonance and the formation of hot spots in the deposited RhITC–Au NPs solution.

Furthermore, an additional enhancement was generated by the use of a Raman reporter displaying an electronic transition in molecular resonance with the laser excitation wavelength (532 nm), leading to the so-called SERRS effect. It has been reported that SERRS can provide additional 10^3 to 10^4 enhancement in comparison to standard SERS experiment, therefore contributing to the high sensitivity and selectivity of the assay.[24,50] In comparison, the Raman spectrum of bare Au NPs recorded before Raman reported encoding (Fig. 4d, black line) appeared featureless.

The functionalization of the Au NPs with anti-P was achieved by passive adsorption of the proteins onto the surface of the nanoparticles. The optimal amount of antibodies, enough to modify the Au NPs surface but not to cause NPs aggregation was calculated through a flocculation stress test.[51,52] Briefly, different volumes (0–50 µL) of anti-P 0.1 mg mL^{-1} were added to 500 µL of Au NPs (OD 1) in presence of borate buffer (BB). Following an incubation at 37 °C for 30 min, 50 µL of NaCl 10% w/v were added to each solution. The optimum volume of anti-P was identified by the preservation of a red colour as close as possible to the original NPs colour prior to surface biomodification. If the volume of added anti-P was too low, a colour transition from red to purple/blue-grey was observed after 10 min, associated to NP aggregation. Upon successful
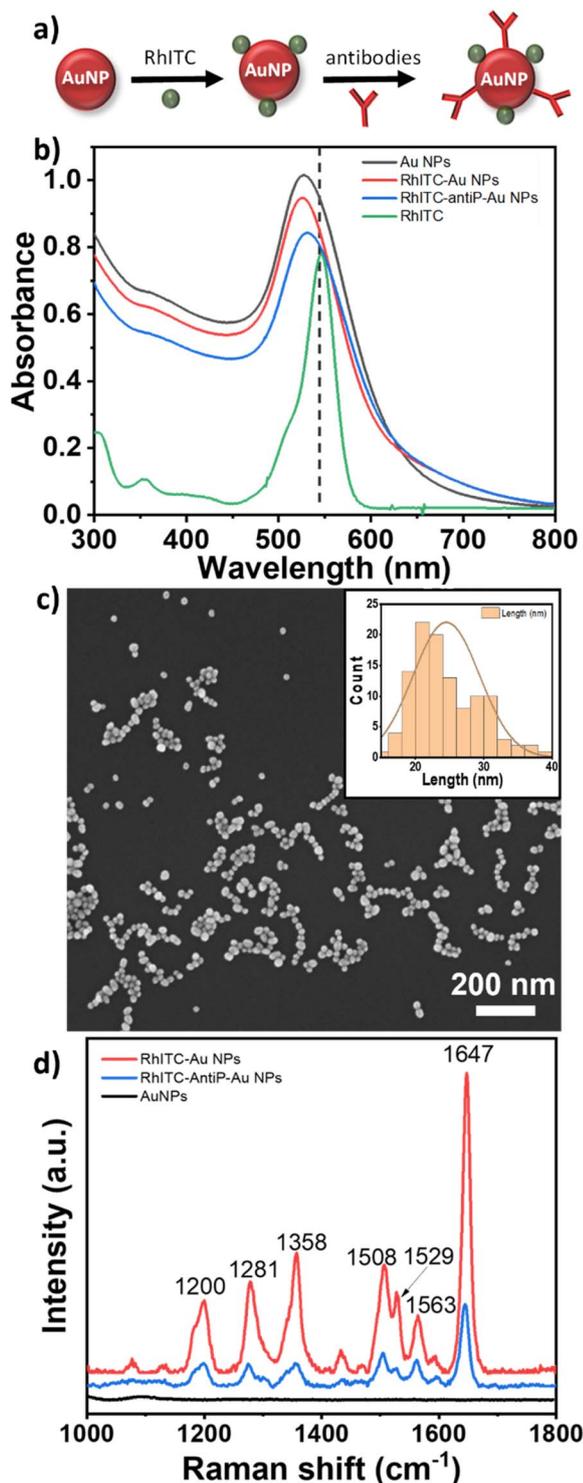
Fig. 4 (a) Schematic of the formation of the RhITC−antiP−Au NPs probe; (b) UV-vis spectra of as prepared Au NPs (black); RhITC−Au NPs (red); RhITC−antiP−Au NPs 1 : 30 (blue); Rhodamine isothiocyanate (green); (c) SEM image of Au NPs solution deposited on SiO₂ wafer with nanoparticle size distribution (inset); (d) Raman spectra of RhITC−Au NPs (red), RhITC−antiP−Au NPs (blue) and Au NPs (black) on a glass-slide, using 532 nm laser, 1% power, 30 s.

Table 1 Comparison of hydrodynamic diameters and zeta potentials of the bare and modified gold nanoparticles

Material	Hydrodynamic diameter (nm)	Zeta potential (mV)
Au NPs	40.8 ± 3.0	−45.1 ± 4.0
RhITC–Au NPs	69.0 ± 7.6	−45.1 ± 2.3
RhITC–antiP–Au NPs	120.6 ± 5.3	−26.6 ± 0.4
AntiP–Au NPs	91.2 ± 7.2	—

surface biomodification, the UV-vis spectrum of the resulting RhITC–antiP–Au NPs showed a shift of the LSPR band of the Au NPs from 525 nm to 532 nm (Fig. 4b, blue line).

Together with LSPR shift, to characterize the probes, zeta potential and DLS were studied. The latter one allowed to attain the hydrodynamic diameter of both bare and modified nanoparticles at 25 °C after 120 s equilibration time between each sample. The results are reported in Table 1, obtained as average of 3 analysed samples for material (3 measurements/sample with 15 runs). Similarly, the results for zeta potential are recorded in same table. It is possible to observe a change (zeta potential increase) in the surface charge only once conjugated with both Raman reporter and antibody.

Optimization of parameters on the antiP–Au NP immunoprobe conjugation and concentration, and other SERRS-LFIA parameters are discussed in detail in the ESI.†

Quantitative analysis of penicillin G using SERRS-LFIA

As explained in detail above, the detection of penicillin G is related to the disappearance of the test line in the LFIA. Prior to conducting quantitative analyses, the "negative" and "positive" visual and SERRS responses of the constructed LFIA platform were tested. Fig. 5a shows a SEM image of the nitrocellulose strip for a negative test, where it was possible to observe the presence of RhITC–antiP–Au NPs at the test line. The corresponding SERRS spectrum in Fig. 5c showed clear response arising from the RhITC–antiP–Au NPs, in line with a negative test, whereby nanoparticles were captured by the antigen penicillin–BSA deposited on the test line. In contrast, Fig. 5b shows a SEM image of a positive test line, whereby only the nitrocellulose was visible. The corresponding Raman spectrum (Fig. 5d) showed only bands attributable to nitrocellulose (1283 cm⁻¹ for $\nu_s(NO_2)$, 1320 cm⁻¹ for $\gamma_w(CH_2)$).[53,54] This was in line with a positive test response where excess RhITC–antiP–Au NPs deposit to the control line only, while the majority of particles bound penicillin G migrating towards the adsorbent pad.

Following the optimization steps described above, the capabilities of the developed SERRS-LFIA platform towards quantitative evaluation of penicillin G in milk was investigated. Fig. 6a shows photographs of LFIA strips obtained with milk samples spiked with standard solutions of penicillin G (0, 0.002, 0.02, 0.2, 2, 20, 200, 500 ppm). Visual discrimination of the
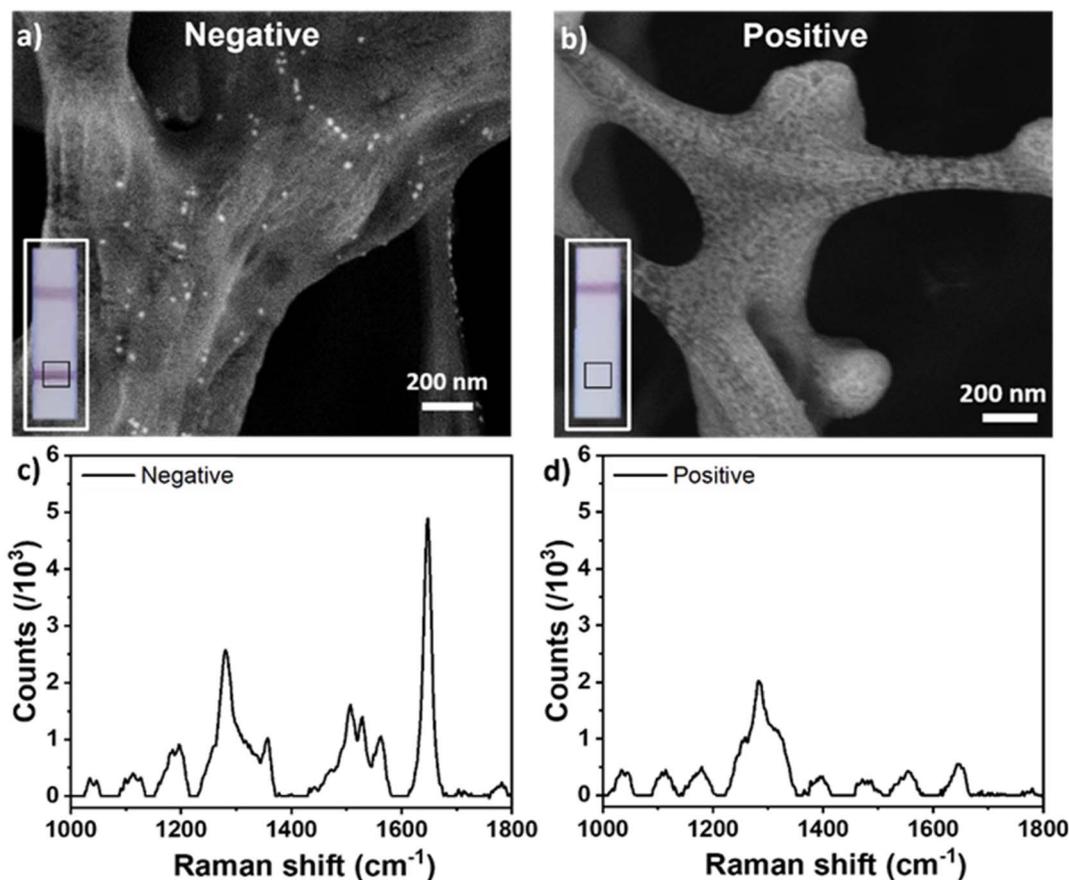
Fig. 5 Photographic images, SERRS spectra and SEM images of SERRS–LFIA in negative (a and c) and positive (b and d) sample.

difference in colour intensity of test lines associated to different penicillin G concentrations resulted difficult, especially for the lowest concentrations. A SERRS analysis was conducted on the test line with different concentrations of penicillin G, for obtaining a quantitative response from the coloured lines. The intensity of reported SERRS spectra increased as the penicillin G concentration decreased from 500 ppm to 0 ppm, following the trend already observed by visual analysis. Fig. 6b shows the correlation between the intensity of the 1647 cm^{-1} RhITC SERRS peak and the concentration of penicillin G in the analysed milk samples.

As expected, the intensity of the diagnostic band decreased with the increase in concentration of penicillin G. During this analysis, it became clear that the reproducibility of SERRS spectra in LFIA strips was low, due to the site-specific nature of Raman and the natural irregularity of the nitrocellulose substrate and the consequent irregular distribution of hot spots. To counteract this effect, during SERRS spectra acquisition individual lateral flow strips were placed in the same position under the Raman microscope. A 50 × 80 μm grid was selected in the middle on each test line, followed by acquisition of nine spectra for each test strip at reproducible locations within the grid. A sigmoidal dependence of the SERRS intensity *vs.* the log of penicillin G concentration was found for the range of penicillin concentration 500 ppm to 0 ppm, as shown in

Fig. 6c; the curve was obtained through a nonlinear regression analysis of the data using a four-parameter logistic equation.[55] The coefficient of variation (CV) for the measurements at different concentrations are available in the Table S2.†

The inter-day reproducibility of the test in milk samples has been assessed and it is reported in Fig. S6.† The fluctuation of measurements expressed by the error bars in the graph could be related not only to the variability strip-to-strip but as well on the preparation of the spiked samples, the variability on the milk sample itself, the laboratory conditions, *etc.*, even while maintaining constant the operator. Still, adding all these, the curve obtained has a correlation coefficient $R^2 = 0.996$ and for each concentration point the CV is <0.3.

In summary, a sensor with a dual detection, visual (qualitative) and SERRS (quantitative) was developed. As shown in Fig. 6a, the visual limit of detection (vLOD) was 20 ppm, while for the SERRS detection the sensitivity of the analysis was defined using the IC$_{50}$, corresponding to the concentration of the analyte producing 50% signal inhibition. For the SERRS-LFIA the IC$_{50}$ is calculated as 1.8 ± 1.5 ppm. Moreover, the dynamic range, expressed as IC$_{10}$–IC$_{90}$, is 0.03–97.5 ppm. According to the European Commission[56] and the Codex Alimentarius[57] the maximum residue limits (MRL) sets for penicillin G in bovine milk is 4 μg kg^{-1}, corresponding to 0.004 ppm, reason why was chosen this range for the measurement.
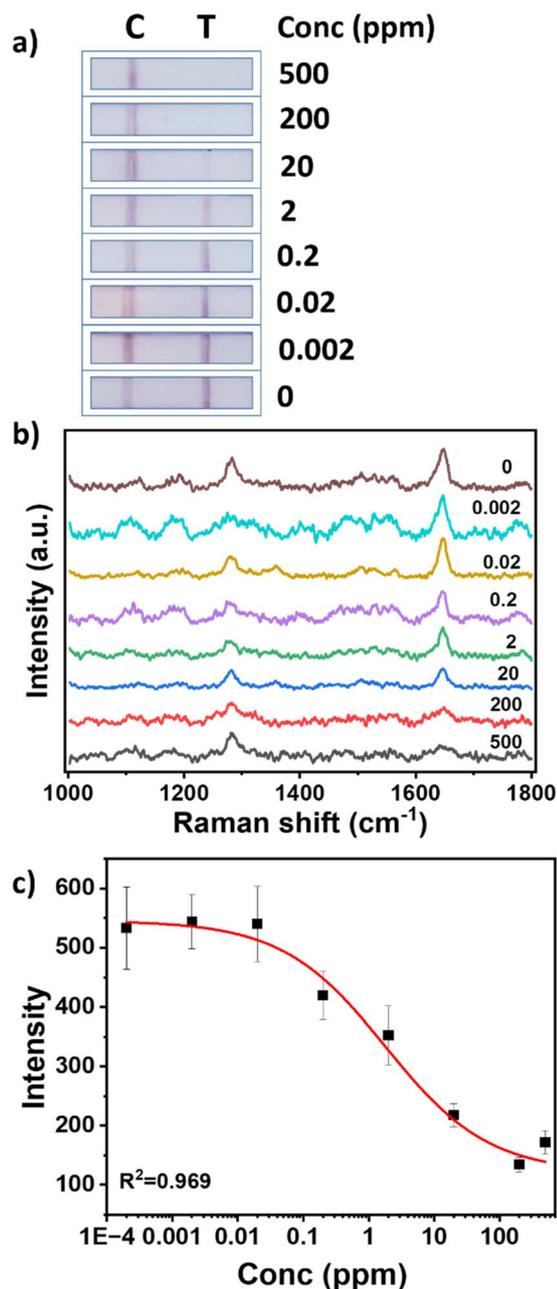
Fig. 6 Quantitative analysis of SERRS-LFIA for penicillin G in milk samples: (a) visual readout of the strips at different concentration levels of penicillin G; (b) SERRS spectra obtained for different levels of concentration of penicillin G; (c) calibration curve obtained considering the intensity of the reference peak for RhITC (1647 cm^{-1}) on 9 points on test line as a function of penicillin G concentration.

Although, the test developed does not result sensitive enough for the MRL and, as well, compared with what already reported in literature (see Table S3†); this is due to a lack in competition at the lower concentrations and so to the affinity of the used antibody–antigen couple, avoiding reaching a higher sensitivity. Still, this result does not affect the objective of the work, which is the development and use of a DIY rapid test with facile fabrication and possibility to use in situation of minimal training or absence of expensive equipment.

Comparison with conventional LFIA test

In order to validate the results obtained with the DIY SERRS-LFIA test, a LFIA test was performed on conventional prepared LFIA strips. These had the T and C lines spotted at 1 μl cm^{-1} by means of a XYZ3050 platform (BioDot, Irvine CA, USA), containing two Biojet Quanti 3000 dispensers for non-contact dispensing. Except for the material deposition, these strips were prepared as already described in the previous sections.

These strips have been used with both antiP–Au NPs and RhITC–antiP–Au NPs. The results obtained are reported in Fig. S7† and they are comparable to those obtained with pen writing. In the conventional deposited strips though, a higher deposition at the front of the line is visible on the test one, followed by a gradation of colour. That needs to be considered on the choice of the area of SERS detection, considering that there will be more variability intra-line. A possibility could be taking different measurement points along the front of the line. For the results reported in ESI,† two points have been considered for the SERRS measurement, one at the front of the line e one in the middle, reason why the error bars are bigger at lower concentrations.

Conclusions

In conclusion, a low cost and versatile DIY approach for the fabrication of LFIA tests was developed. The qualitative capabilities of the test were enhanced by incorporation of a Raman reporter, which was crafted on the Au NPs immunoprobe allowing quantitative detection. The viability of the approach was tested through development of a competitive SERRS-LFIA test for detection of penicillin G in milk. The test gave a visual LOD of 20 ppm and range of quantification (IC$_{10}$–IC$_{90}$) of 0.03–97.5 ppm. Comparison with traditional and more costly LFIA fabrication methods showed that the developed method is viable and has the potential to be extended to detection of other antibiotics and a wide range of analytes. The presented DIY approach gives a simple and flexible method to deposit biomaterials on nitrocellulose support and paper substrates thus opening the way to development of POC tests that can be prepared and used *in situ*, with minimal training, using small volume of reagents and without the need of expensive equipment.

In addition, to provide flexibility and cost-effectiveness, the possibility to integrate the LFIA strip to a portable Raman spectrometer offers a huge potential in point-of-care testing in real-world applications, especially in fields like food safety, environmental monitoring, or clinical diagnostics.

Data availability

The data presented in this article are available from the author upon reasonable request.

Author contributions

The manuscript was written through contributions of all authors. All authors have given approval to the final version of the manuscript.

Conflicts of interest

There are no conflicts to declare.

Acknowledgements

References

1 S. Liu, R. Cao, J. Wu, L. Guan, M. Li, J. Liu and J. Tian, *Sens. Actuators, B*, 2019, **285**, 529–535.

2 A. Ghosale, K. Shrivas, R. Shankar and V. Ganesan, *Anal. Chem.*, 2017, **89**, 776–782.

3 Y. L. Han, J. Hu, G. M. Genin, T. J. Lu and F. Xu, *Sci. Rep.*, 2014, **4**, 4872.

4 H. Jia, J. Wang, X. Zhang and Y. Wang, *ACS Macro Lett.*, 2014, **3**, 86–90.

5 R. Amin, F. Ghaderinezhad, L. Li, E. Lepowsky, B. Yenilmez, S. Knowlton and S. Tasoglu, *Anal. Chem.*, 2017, **89**, 6351–6357.

6 A. J. Bandodkar, W. Jia, J. Ramírez and J. Wang, *Adv. Healthcare Mater.*, 2015, **4**, 1215–1224.

7 J. R. Camargo, L. O. Orzari, D. A. G. Araújo, P. R. de Oliveira, C. Kalinke, D. P. Rocha, A. Luiz dos Santos, R. M. Takeuchi, R. A. A. Munoz, J. A. Bonacin and B. C. Janegitz, *Microchem. J.*, 2021, **164**, 105998.

8 F. C. Loghin, J. F. Salmerón, P. Lugli, M. Becerer, A. Falco and A. Rivadeneyra, *Chemosensors*, 2021, **9**, 264.

9 V. Soum, H. Cheong, K. Kim, Y. Kim, M. Chuong, S. Ryeon Ryu, P. K. Yuen, O.-S. Know and K. Shin, *ACS Omega*, 2018, **3**, 16866–16873.

10 S. Choi, J.-H. Lee, J.-S. Choi and H.-I. Jung, *Anal. Methods*, 2015, **7**, 1834–1842.

11 J. Nie, Y. Zhang, L. Lin, C. Zhou, S. Li, L. Zhang and J. Li, *Anal. Chem.*, 2012, **84**, 6331–6335.

12 N. Dossi, S. Petrazzi, F. Terzi, R. Toniolo and G. Bontempelli, *Talanta*, 2019, **199**, 14–20.

13 Z. Li, H. Liu, X. He, F. Xu and F. Li, *TrAC, Trends Anal. Chem.*, 2018, **108**, 50–64.

14 Y. Liu, L. Zhan, Z. Qin, J. Sackrison and J. C. Bischof, *ACS Nano*, 2021, **15**, 3593–3611.

15 Q.-Y. Xie, Y.-H. Wu, Q.-R. Xiong, H.-Y. Xu, Y.-H. Xiong, K. Liu, Y. Jin and W.-H. Lai, *Biosens. Bioelectron.*, 2014, **54**, 262–265.

16 J. Deng, M. Yang, J. Wu, W. Zhang and X. Jiang, *Anal. Chem.*, 2018, **90**, 9132–9137.

17 A. V. Orlov, J. A. Malkerov, D. O. Novichikhin, S. L. Znoyko and P. I. Nikitin, *Food Chem.*, 2022, **383**, 132427.

18 M. R. Akanda, H.-A. Joung, V. Tamilavan, S. Park, S. Kim, M. H. Hyun, M.-G. Kim and H. Yang, *Analyst*, 2014, **139**, 1420–1425.

19 R. Wang, K. Kim, N. Choi, X. Wang, J. Lee, J. H. Jeon, G. Rhie and J. Choo, *Sens. Actuators, B*, 2018, **270**, 72–79.

20 K. Kim, L. Kashefi-Kheyrabadi, Y. Joung, K. Kim, H. Dang, S. G. Chavan, M.-H. Lee and J. Choo, *Sens. Actuators, B*, 2021, **329**, 129214.

21 Z. Wang, S. Zong, L. Wu, D. Zhu and Y. Cui, *Chem. Rev.*, 2017, **117**, 7910–7963.

22 D. Quesada-González and A. Merkoçi, *Biosens. Bioelectron.*, 2015, **73**, 47–63.

23 R. Pilot, R. Signorini, C. Durante, L. Orian, M. Bhamidipati and L. Fabris, *Biosensors*, 2019, **9**, 57.

24 G. McNay, D. Eustace, W. E. Smith, K. Faulds and D. Graham, *Appl. Spectrosc.*, 2011, **65**, 825–837.

25 R. Fan, S. Tang, S. Luo, H. Liu, W. Zhang, C. Yang, L. He and Y. Chen, *Molecules*, 2020, **25**, 5249.

26 X. Fu, Z. Cheng, J. Yu, P. Choo, L. Chen and J. Choo, *Biosens. Bioelectron.*, 2016, **78**, 530–537.

27 K. V. Serebrennikova, N. A. Byzova, A. V. Zherdev, N. G. Khlebtsov, B. N. Khlebtsov, S. F. Biketov and B. B. Dzantiev, *Biosensors*, 2021, **11**, 510.

28 L. Shi, L. Xu, R. Xiao, Z. Zhou, C. Wang, S. Wang and B. Gu, *Front. Microbiol.*, 2020, **11**, 596005.

29 J. Hwang, S. Lee and J. Choo, *Nanoscale*, 2016, **8**, 11418–11425.

30 T. Bai, M. Wang, M. Cao, J. Zhang, K. Zhang, P. Zhou, Z. Liu, Y. Liu, Z. Guo and X. Lu, *Anal. Bioanal. Chem.*, 2018, **410**, 2291–2303.

31 D. Zhang, L. Huang, B. Liu, H. Ni, L. Sun, E. Su, H. Chen, Z. Gu and X. Zhao, *Biosens. Bioelectron.*, 2018, **106**, 204–211.

32 *Sales of Veterinary Antimicrobial Agents in 31 European Countries in 2022 – Trends from 2010 to 2022 – Thirteenth ESVAC Report*, 2023.

33 J. M. Mitchell, M. W. Griffiths, S. A. Mcewen, W. B. Mcnab and A. J. Yee, *J. Food Prot.*, 1998, **61**, 742–756.

34 *Sales of Veterinary Antibiotics in Ireland during 2022*, Health Products Regulatory Authority, 2023.

35 M. I. Bailón-Pérez, A. M. García-Campaña, M. del Olmo-Iruela, L. Gámiz-Gracia and C. Cruces-Blanco, *J. Chromatogr. A*, 2009, **1216**, 8355–8361.

36 F. Tasci, H. S. Canbay and M. Doganturk, *Food Control*, 2021, **127**, 108147.

37 J.-I. Kim, J.-M. Park, J.-Y. Noh, S.-J. Hwang, M.-J. Kang and J.-C. Pyun, *Chemosphere*, 2016, **143**, 64–70.

38 T. Romero, S. Van Weyenberg, M. P. Molina and W. Reybroeck, *Int. Dairy J.*, 2016, **62**, 39–42.

39 O. Çelik, Y. Saylan, I. Göktürk, F. Yılmaz and A. Denizli, *Talanta*, 2023, **253**, 123939.

40 J. Pietschmann, D. Dittmann, H. Spiegel, H.-J. Krause and F. Schröper, *Foods*, 2020, **9**, 1773.

41 M. Gamella, S. Campuzano, F. Conzuelo, M. Esteban-Torres, B. de las Rivas, A. J. Reviejo, R. Muñoz and J. M. Pingarrón, *Analyst*, 2013, **138**, 2013–2022.

42 P. Cliquet, E. Cox, C. Van Dorpe, E. Schacht and B. M. Goddeeris, *J. Agric. Food Chem.*, 2001, **49**, 3349–3355.

43 J. Turkevich, P. C. Stevenson and J. Hillier, *Discuss. Faraday Soc.*, 1951, **11**, 55.

44 G. Frens, *Nature, Phys. Sci.*, 1973, **241**, 20–22.

45 L. Anfossi, F. Di Nardo, A. Russo, S. Cavalera, C. Giovannoli, G. Spano, S. Baumgartner, K. Lauter and C. Baggiani, *Anal. Bioanal. Chem.*, 2019, **411**, 1905–1913.

46 L. Anfossi, M. Calderara, C. Baggiani, C. Giovannoli, E. Arletti and G. Giraudi, *Anal. Chim. Acta*, 2010, **682**, 104–109.

47 P. Hildebrandt and M. Stockburge, *J. Phys. Chem.*, 1984, **88**, 5765–6080.

48 L. Polavarapu, A. L. Porta, S. M. Novikov, M. Coronado-Puchau and L. M. Liz-Marzán, *Small*, 2014, **10**, 3065–3071.

49 L. Blanco-Covián, V. Montes-García, A. Girard, M. T. Fernández-Abedul, J. Pérez-Juste, I. Pastoriza-Santos, K. Faulds, D. Graham and M. C. Blanco-López, *Nanoscale*, 2017, **9**, 2051–2058.

50 A. Królikowska, *Electrochim. Acta*, 2013, **111**, 952–995.

51 D. K. Toubanaki, M. Margaroni, A. Prapas and E. Karagouni, *Sci. Rep.*, 2020, **10**, 6529.

52 S. Cavalera, A. Russo, E. A. Foglia, S. Grazioli, B. Colitti, S. Rosati, C. Nogarol, F. Di Nardo, T. Serra, M. Chiarello, C. Baggiani, G. Pezzoni, E. Brocchi and L. Anfossi, *Talanta*, 2022, **240**, 123155.

53 D. S. Moore and S. D. McGrane, *J. Mol. Struct.*, 2003, **661–662**, 561–566.

54 K. Castro, S. F.-O. de Vallejuelo, I. Astondoa, F. M. Goñi and J. M. Madariaga, *J. Raman Spectrosc.*, 2011, **42**, 2000–2005.

55 J. W. A. Findlay, W. C. Smith, J. W. Lee, G. D. Nordblom, I. Das, B. S. DeSilva, M. N. Khan and R. R. Bowsher, *J. Pharm. Biomed. Anal.*, 2000, **21**, 1249–1273.

56 *Commission Regulation (EU) No 37/2010 of 22 December 2009 on Pharmacologically Active Substances and Their Classification Regarding Maximum Residue Limits in Foodstuffs of Animal Origin*, vol. L 15.

57 *Codex Alimentarius – Maximum Residue Limits (MRLs) and Risk Management Recommendations (RMRs) for Residues of Veterinary Drugs in Foods*, vol. CX/MRL 2-2021.